Large deformation finite element modeling of progressive failure leading to spread in sensitive clay slopes

Rajib Dey[1], Bipul Hawlader[2], Ryan Phillips[3] and Kenichi Soga[4]

[1]PhD Candidate, Department of Civil Engineering, Memorial University of Newfoundland, St. John's, Newfoundland, Canada A1B 3X5
Tel: +1 (709) 864-7961, E-mail: rdey@mun.ca

[2]**Corresponding Author:** Associate Professor, Department of Civil Engineering, Memorial University of Newfoundland, St. John's, Newfoundland, Canada A1B 3X5
Tel: +1 (709) 864-8945   Fax: +1 (709) 864-4042   E-mail: bipul@mun.ca

[3]Principal Consultant, C-CORE, Captain Robert A Bartlett Building, Morrissey Road, St. John's, Newfoundland, Canada A1B 3X5
Tel: +1 (709) 864-8371   Fax: +1 (709) 864-4706   E-mail: ryan.phillips@ c-core.ca

[4]Professor, University of Cambridge, Department of Engineering, Trumpington Street, Cambridge, UK CB2 1PZ
Tel: +44 1223 332713 Fax: +44 1223 332913   E-mail: ks207@cam.ac.uk

Abstract

The occurrence of large landslides in sensitive clays, such as spreads, can be modeled by progressive development of large inelastic shear deformation zones (shear bands). The main objective of the present study is to preform large deformation finite element (FE) modeling of sensitive clay slopes to simulate progressive failure and dislocation of failed soil mass using the Coupled Eulerian Lagrangian (CEL) approach available in Abaqus FE software. The degradation of undrained shear strength with plastic shear strain (strain-softening) is implemented in Abaqus CEL, which is then used to simulate the initiation and propagation of shear bands due to river bank erosion. The formation of horsts and grabens and dislocation of soil masses that lead to large-scale landslides are simulated. This FE model explains the displacements of different blocks in the failed soil mass and also the remoulding of soil around the shear bands. The main advantages of the present FE model over other numerical models available in the literature are that it can simulate the whole process of progressive failure leading to spread. The FE results are consistent with previous conceptual models proposed from field observations. The parametric study shows that, depending upon geometry and soil properties, toe erosion could cause three types of shear band formation: (i) only a horizontal shear band without any global failure, (ii) global failure of only one block of soil, (iii) global failure of multiple blocks of soil in the form of horsts and grabens.

Key words: landslides, sensitive clay, progressive failure, large deformation, finite element modeling, shear band, horst and grabens

Introduction

Large-scale landslides in sensitive clays are common in Eastern Canada and Scandinavia. Most of these slides are progressive in nature. The post-peak softening of sensitive clays is

2

considered as one of the main reasons of progressive failure. The failure occurs quite rapidly, essentially in undrained conditions (Locat et al., 2013). Based on initiation and progression of the sliding surfaces or shear bands, the failure of slopes can be divided into two categories, namely upward and downward progressive failures. Upward progressive failure might be initiated due to excavation, erosion or small slides in the river bank slopes (Quinn et al., 2007; Locat et al., 2008; Demers et al., 2013). On the other hand, downward progressive failure could be triggered by vertical loading or pile driving in the upslope area (Bernander, 2000; Gylland et al, 2010). The numerical modeling of upward progressive failure is presented in this paper. It is to be noted here that the propagation of shear band has been identified as one of the key factors for modelling different types of failure, such as catastrophic failure of mild submarine slopes and progressive failure of embankments (Potts et al., 1990; Puzrin et al., 2004; Puzrin and Germanovich, 2005; Gauer et al., 2005; Kvalstad et al., 2005). The focus of the present study is to analyze the failure of sensitive clay slopes under undrained conditions.

Landslides in sensitive clays could be in the form of multiple retrogressive, translational progressive or spreads (Tavenas, 1984; Karlsrud et al., 1984). According to Fortin et al. (2008), 42% of large landslides which occurred in Eastern Canada can be categorized as spreads. Many spread failures such as Sköttorp landslide in Sweden (Odenstad, 1951) and the landslides occurred in Quebec including the 1989 Saint-Liguori landslide (Grondin and Demers, 1996), Saint-Ambroise-de-Kildare landslide (Carson, 1977), Saint-Barnabé-Nord slide (Locat et al., 2008) are reported to be triggered by erosion at the toe of the slope (Bernander, 2000; Locat et al., 2008; Quinn et al., 2007; Locat et al., 2011), even though it is very difficult to identify the true triggering mechanisms. The spread type of failures could be explained by the progressive failure mechanisms (Locat et al., 2013).

Field observations show that the progressive failure propagating in upslope direction is initiated by formation of a quasi-horizontal shear band from the toe of the slope (Locat et al., 2011; 2013). Due to significant displacement, the soil layer above this shear band might dislocate into a number of soil blocks in the form of horsts and grabens (Fig. 1). The shear strains are mainly concentrated around the surfaces of the horsts and grabens with minimal strains inside these blocks. Moreover, once the failure surfaces are developed, the horsts and grabens displace almost laterally on the initially developed quasi-horizontal shear band that results in spread. This process is shown schematically in Figure 2. Very large strains and displacements are developed around the shear bands and therefore it should be modeled as a large deformation problem.

To explain upward progressive failure and spreads, the presence of a horizontal weak layer/surface was recognized by researchers several decades ago (Odenstad, 1951; Carson, 1977). Examining field evidences, in the recent studies (e.g. Locat et al., 2008; 2011; 2013; Quinn et al., 2011) it is shown that the initial horizontal shear band might form due to erosion, excavation or small slides near the bank. Locat et al. (2011) demonstrated the mechanisms of quasi-horizontal shear band formation for an idealized condition in an infinite slope. An external force parallel to the ground surface is applied near the toe above the predefined shear zone. The variation of shear stress, in relation to shear strength, with distance from the point of load is discussed. Locat et al. (2013) extended their work (Locat et al., 2011) through numerical modeling using PLAXIS 2D (PLAXIS, 2011) and BIFURC (Jostad and Andresen, 2002) FE programs. In this decoupled modeling, the initial stresses of soil are calculated using the PLAXIS 2D with the Mohr-Coulomb model. The calculated stresses from PLAXIS are then used in BIFURC to simulate the initiation and progression of a quasi-horizontal shear band, simply by pulling the top of the predefined shear zone at the toe of slope. While these initial attempts partly explain the mechanisms involve in shear

4

band formation, the complete failure processes were not simulated. These studies have some limitations. They could simulate the formation of quasi-horizontal shear band only, because the soil above the shear zone is assumed to be elastic. With the applied force, the length of the shear band increases along the predefined shear zone. However, in reality another shear band might form from the horizontal shear band that might propagate to the ground surface resulting in global failure of the slope as discussed in the following sections. As it is not possible to model this with elastic soil properties above the shear zone, they assumed that the global failure occurs when it reaches the active failure condition. With their numerical techniques, the formation of subsequent horsts and grabens could not be simulated.

Quinn et al. (2011) used the concepts of linear elastic fracture mechanics (FM) and proposed a model for development of shear band in a simplified slope with a vertical cut. The critical length required to initiate the propagation of the shear band was calculated using the approach of Palmer and Rice (1973). They hypothesized that the failure of the slope would occur when the length of the shear band is sufficiently large such that the downward unbalanced force causes active shear failure. The authors also used the same concept to analyze the stability of the slope with additional stresses due to earthquake loading (Quinn et al., 2012). They also conducted elastic FE analysis to validate some of their assumptions.

Norwegian Geotechnical Institute (NGI) (Jostad and Andresen, 2002; Andresen and Jostad, 2004; Andresen and Jostad, 2007; Gylland et al., 2010) also analyzed progressive failure of slopes developing the computer program BIFURC. However, none of these numerical techniques could simulate the complete process of upward progressive failure.

Recognizing the fact that the progressive failure of slopes involves large deformation, the Coupled Eulerian Lagrangian (CEL) approach in Abaqus FE software is used in the present FE

analyses. The paper is organized in the following way. First, the FE modeling in Abaqus CEL is presented. A model that represents the variation of undrained shear strength (s_u) with shear strain is presented in the second part. In the third part, the formation of shear bands and horsts and grabens is presented. Finally, a parametric study is conducted to show the effects of some soil parameters and the slope geometry.

Problem Definition

The geometry of the 'base case' slope considered in this study is shown in Fig. 3. The river bank has a slope, β of 30° and the ground surface is horizontal. There is a crust of overconsolidated clay near the face of the slope and below the ground surface. The thickness of the crust below the level ground surface is H_c. Under the crust there is a thick layer of sensitive clay (thickness H_{st}) followed by a base layer of stiff clay. It is assumed that the base layer is very thick; however, in the FE analyses only 3 m of this layer is modeled as it does not have significant effect on the results, which has been verified by an analysis with a 10 m thick base layer. The geometry considered here is an idealized section of river banks in Eastern Canada where spread failures have occurred (Locat et al., 2011; Quinn et al., 2012). Note that change in geometry and soil properties, including the property of base layer, might alter the failure pattern.

For simplicity the groundwater table is assumed to be located at the ground surface and the river is full. Potential long-term failure of the riverbank is not considered. It is assumed that the upward progressive failure is initiated by erosion and/or excavation of the river bank. In the FE analyses, the erosion or excavation is modeled by removing a block of soil near the toe of the slope as shown by the shaded zone in Fig. 3. In the following sections this block will be referred as the "eroded block." It is also assumed that the erosion or excavation occurs relatively fast such that the deformation/failure of remaining soil occurs in undrained condition. The length of the soil domain

in the present FE model is 200 m and therefore no significant effects on the results are expected from the right boundary.

Finite Element Modeling

The elasto-plastic FE analysis is a powerful alternative approach for slope stability analysis over conventional limit equilibrium methods. Most of the FE models available in the literature for slope stability analysis are developed in a Lagrangian framework (e.g. Griffiths and Lane, 1999; Loukidis et al., 2003). One of the main disadvantages of this type of model is that a significant mesh distortion occurs around the failure planes. The non-convergence of the solution due to significant mesh distortion is considered as one of the conditions of failure in some studies (e.g. Griffith and Lane, 1999). In order to overcome these issues, the CEL approach in Abaqus 6.10 EF1 is used in this study. In CEL, the mesh is fixed and soil as Eulerian material flow through the fixed mesh. Therefore, numerical issues related to mesh distortion or mesh tangling, even at very large strains, are not expected anywhere including the zones around the failure planes. Note that Abaqus CEL has been used in previous studies for other applications such as quasi-static penetration of spudcan foundations and offshore pipelines (Qiu et al., 2011; Tho et al., 2012; Dutta et al., 2015). Its performance has also been validated by comparing the results with the remeshing and interpolation technique with small strain (RITSS) for static and dynamic problems (Tian et al., 2011; Wang et al., 2013)

The CEL framework allows only three-dimensional modeling, and therefore the analyses are performed with only one element length in the out of plane direction. For the 'base case' analysis, 0.5 m × 0.5 m mesh is used. However, analyses are also performed for different mesh sizes and a mesh independent modeling technique is presented. The FE model consists of three parts: (i) soil,

(ii) eroded block and (iii) void space. The eroded block is modeled as a rigid body in the Lagrangian framework, which makes the model computationally efficient, while the soil is modeled as an Eulerian material using EC3D8R 8-noded brick elements. A void space (efghij) is created above the soil as shown in Fig. 3 to accommodate displaced soil. The soil and voids for the initial condition are created using the Eulerian Volume Fraction (EVF) tool available in Abaqus. For clay, EVF=1 meaning that the elements are filled with Eulerian material (clay) while EVF=0 for the void space. Zero velocity boundary conditions are applied normal to the bottom and all the vertical faces of the domain. No velocity boundary condition is applied at the soil-void interface (efgh in Fig. 3) so that the soil can move into the void space when needed. Unbonded smooth interface condition between the eroded block and clay is used.

The numerical analysis consists of two steps of loading. Keeping the eroded block fixed, the geostatic load is applied in the first step to bring the soil to an in-situ stress condition under $K_0=1$. The initial effective stresses influence the failure of the slope (Lo and Lee, 1973; Locat et al., 2013) and therefore analyses with different initial effective stress conditions need to be performed. The slope is stable in the geostatic step for the conditions analyzed here, even though some shear stress (less than peak undrained shear strength) develops especially near the river bank. In the second step, the eroded block is displaced laterally (Δ) up to 30.75 m at a constant speed (v_e) of 0.05 m/s to the left applying a displacement boundary condition at the reference point of the rigid body. The speed 0.05 m/s is low enough to maintain quasi-static conditions during the analyses with the 0.5-m mesh, as the analysis at a slower speed (v_e=0.01 m/s) does not show any significant change in the failure pattern. However, the computational time for this slow speed is very high and therefore all the analyses presented in the following sections are performed at v_e=0.05 m/s unless otherwise mentioned. Note that, analyses are also performed by replacing the eroded block with soil of same

8

properties of the crust and sensitive clays and found that the slope is stable after the geostatic step. This implies that the movement of the eroded block represents the effect of erosion on a stable slope.

Undrained shear strength of soil

Laboratory tests (e.g. Tavenas et al., 1983; Bjerrum and Landva, 1966; Bernander, 2000) show that the undrained shear strength of sensitive clay decreases with plastic shear strain. Following Anastasopoulos et al. (2007), it is assumed that equal shear strains develop throughout the whole depth of the soil specimen until the peak. After that, the shear strain is localized in a very small region along the shear band. The shear strain could be calculated if the thickness of the shear band is known; however, the proper estimation of shear band thickness is very difficult in laboratory experiments or in the field. Therefore, shear displacement is used to define the post-peak softening curve while shear strain is used in the pre-peak region. It is to be noted here that previous authors (e.g. Quinn et al., 2011) also recommended to use relative displacement along the shear band after the peak and the strain concepts for the pre-peak elastic part of the stress-strain curve.

Figure 4 shows the stress-strain behaviour of sensitive clay used in the present FE analysis. The linear elastic pre-peak segment (line *oa* in Fig. 4) is defined by undrained Young's modulus (E_u) and Poisson's ratio (v_u). The peak undrained shear strength (s_{up}) is mobilized at point *a* and remains constant up to point *b* for a displacement of δ_{pc} from point *a*. The undrained shear strength at completely remoulded (stirred) condition (s_{ur}) can be measured in laboratory. However, Bernander (2000) could not find relevance of s_{ur} in post-slide investigations and therefore recommended an undrained shear strength s_{uR} ($>s_{ur}$) for progressive failure analysis that mobilizes in shear bands at a considerable shear displacement.

The shear strength degradation curve (*bcd*) is defined by the following exponential function.

$$s_u = \left[\frac{1}{S_t} + \left(1 - \frac{1}{S_t}\right) e^{-3\delta/\delta_{95}} \right] s_{up} \qquad (1)$$

where s_u is the mobilized undrained shear strength; $\delta = \delta_t - (\delta_e + \delta_{pc})$ with δ_e and δ_t are the elastic and total shear displacements, respectively; δ_{95} is the value of δ at which the undrained shear strength is reduced by 95% of (s_{up}-s_{uR}) and $S_t = s_{up}/s_{uR}$. Equation (1) is a modified form of strength degradation equation proposed by Einav and Randolph (2005), but in terms of displacement along the shear band. As it is an exponential curve, s_u up to $2\delta_{95}$ is defined by Eq. (1). After that a linear relationship (line *de*) is used to decrease s_u to a constant $s_{u(ld)}$ at δ_{ld}. Assuming simple shear condition, the plastic shear strain (γ^p) can be calculated as $(\delta_t-\delta_e)/t$, where t is the thickness of the soil element. In FE analysis, the variation of yield strength (=2s_u) is defined as a function of plastic shear strain, which is calculated assuming $t = t_{FE}$, where t_{FE} is the thickness of the cubical EC3D8R elements. The von Mises yield criterion is adopted.

Table 1 shows the geotechnical parameters used in this study. These parameters are estimated from laboratory tests, interpretation of test data, constitutive model development and numerical studies on landslides in sensitive clays available in the literature (e.g. Tavenas et al., 1983; Bernander, 2000; Leroueil, 2001; Locat et al., 2008; Quinn, 2009; Quinn et al., 2011; Locat et al., 2011 and 2013). Tavenas et al. (1983) presented experimental results of undrained shear strength behaviour of Champlain sea clays from 7 different sites in Quebec, Canada. Equation (1), with the model parameters in Table 1, fits these experimental results well.

The presence of fissures might affect the apparent shear strength of the crust. The distribution of fissures and their continuity would govern the shear resistance in a slope stability analysis. In the present study, the effects of fissures are not modeled rather an average undrained shear strength is assumed for the crust.

Results of Base Case Analysis

Propagation of shear band

The strain localization and formation of shear bands are the key issues in landslides in sensitive clays. Figure 5 shows the development of shear stress (τ_c) and equivalent plastic shear strain (PEEQVAVG) with displacement of eroded block (Δ). PEEQVAVG represents the integration of plastic deviatoric strain rate tensor over the period of analysis, which is related to plastic shear strain in simple shear condition (γ^p) as PEEQVAVG=$\gamma^p/\sqrt{3}$. The shear strain concentrates mainly in one layer elements and a shear band is formed that propagates horizontally with increasing Δ. Figure 5a shows the variation of PEEQVAVG when Δ=0.1 m. For the parameters listed in Table 1, s_u=s_{u95} at PEEQVAVG=0.035 (see Eq. 1, and definition of strain discussed above). For the ease of discussion, let us define the zone where PEEQVAVG$\geq$0.035 (i.e. $s_u\leq s_{u95}$, Section c-d-e in Fig. 4) as 'residual shear band' because significantly large plastic strain accumulates in this zone. The zone where $s_{u95}<s_u< s_{up}$ (Section b-c in Fig. 4) is defined as 'softening zone.' Figure 5(a) shows that a 21.5 m long horizontal residual shear band is formed when Δ=0.1 m.

Figure 5(b) shows the variation of shear stress (τ_c) along the shear band for Δ=0.05, 0.06, 0.075 and 0.1 m. In order to explain the process, consider the variation of τ_c for Δ=0.1 m. The maximum τ_c of 37.5 kPa (i.e. s_{up}) is mobilized at 25 m from the vertical face of the eroded block. Between 0 and 25 m, $\tau_c\leq$37.5 kPa (i.e. $\tau_c\leq s_{up}$), meaning that the s_u along this length is in the post-peak softening zone (Section *be* in Fig. 4), because $\gamma^p \geq \gamma_c^p$ as shown in Fig. 5(a). In the first 21.5 m length of residual shear band $\tau_c\leq s_{u95}$. The left side of the peak (21.5–25 m) where τ_c increases from s_{u95} to s_{up} represents the softening zone. After 25 m, τ_c is again less than s_{up}. In this zone the yield strength is not mobilized and it represents the pre-yield behaviour (line *oa* in Fig. 4). At a very

11

large distance, τ_c reduces to zero as the ground surface is horizontal. The pattern of τ_c for other

values of Δ is similar, although the location of maximum τ_c moves to the right with increasing Δ.

As an example, for $\Delta=0.1$ m the maximum τ_c is at 25 m while it is at 11 m for $\Delta=0.06$ m.

In the following sections, the discussion is mainly focused on residual shear band ($\gamma^p \geq \gamma_{95}^p$)

formation and propagation.

Development of spread failure

Figure 6 shows the formation of shear bands for six values of Δ during the displacement of the

eroded block to $\Delta=30.75$ m. A horizontal shear band f_1 is formed when $\Delta=0.5$ m. The maximum

PEEQVAVG is developed near the toe, which gradually decreases with horizontal distance. The

initiation of a shear band near the toe and its propagation in sensitive clays almost in the horizontal

direction are reported in previous studies (Locat, 2007; Locat et al., 2008 and 2013; Fortin-

Rhéaume, 2013). At $\Delta=0.65$ m, a curved shear band f_2 starts to form from point P_1 when the length

of f_1 is 88.5 m. The band f_2 propagates up to the ground surface at $\Delta=0.75$ m (Fig. 6b). With further

displacement of the eroded block, the soil mass M1 slides along a failure plane formed by the shear

bands f_1 and f_2. At this same time, M1 also rotates in the clockwise direction and therefore a gap

is formed between M1 and the eroded block near the top as shown in Fig. 6(c). Because of this

lateral displacement and rotation of M1, settlement occurs where f_2 intersects the ground surface.

As significant deformation occurs, the extent of the plastic shear strain zone around the failure

plane also increases (compare PEEQVAVG in Figs. 6b and 6c). Near the toe of the slope, multiple

surfaces of high plastic shear strain develop. At $\Delta=4.5$ m, another shear band f_3 starts to form in

the sensitive clay layer from the intersection of f_2 and the bottom of the crust (point P_2). The band

f_3 propagates further toward deeper depths and at $\Delta=5.95$ m it joins the initially developed shear

12

band f_1. At this stage, a soil mass (M2) bounded by the shear bands f_1, f_2 and f_3 forms a horst. As undrained (ϕ=0) condition is used, the tip of the simulated horst is approximately 90° although in the field this angle is typically close to 60° (Carson, 1979; Locat et al., 2011). A better soil model might be able to simulate this shape.

As the displacement continues, another shear band f_4 starts to form from point P$_3$ on f_1 at Δ=10.5 m. The shear band f_4 reaches to the ground surface at Δ=12.15 m (Fig. 6d). Another soil mass M3 bounded by the shear bands f_1, f_3 and f_4 fails, which is commonly known as a graben. This process will be continued (Figs. 6e & f) until: (i) a strong or less sensitive soil layers are encountered in the upward (right) direction, (ii) the movement of the soil mass M1 is obstructed in the downward (left) side, and/or (iii) length of f_1 is not sufficient for formation of another horst. Let us define the extent of failure (L_{ex}) as the lateral distance between the initial position of crest of the slope and the point where the last shear band intersects the ground surface. In this case, the displacement of the eroded block is stopped at Δ=30.75 m and L_{ex}=73 m is obtained (see Fig. 6f).

Figure 7 shows the instantaneous velocity vectors of soil elements for four different stages. As shown in Fig. 6(b), a complete failure plane is developed when the shear band f_2 propagates up to the ground surface at Δ=0.075 m. After that the soil mass M1 slides on this failure plane. The instantaneous velocities of soil particles at Δ=9.15 m are shown in Fig. 7(a). The velocities of soil particles near the face of the slope are less than those of the particles near the failure plane, which causes the rotation of M1 as discussed above. Due to movement of M1, the lateral support on the remaining soil is reduced. Moreover, s_u in the shear bands f_1 under the block M2 in Fig. 6(c) is significantly reduced because of increase in plastic shear strain. The combined effects of these two factors results in formation of shear band f_3 and the horst M2 at Δ=5.95 m (Fig. 6c). The velocities of soil elements at Δ=11.15 m are shown in Fig 7b. As expected, the velocities of the soil elements

in M1 are higher than those in M2. The soil particles in M1 slides on the shear band f_2 and a crater is formed. On the other hand, the horst M2 moves laterally to the left. The lateral movement of M2 reduces the support on remaining soil that results in formation of the shear band f_4 and the graben M3. The velocity vectors at Δ=12.55 m are shown in Fig. 7(c). The velocities of soil particles gradually decrease from M1 to M3. This process is continued with increasing Δ, and the mechanism involved in formation of each horst and graben can be explained in the same way. For a large value of Δ=25.35 m (Fig. 7d), the movements of soil masses M1 to M4 are almost horizontal, while the graben M5 moves downward left. Moreover, as expected, the velocity of M1 is the highest and M5 is the lowest at this stage. Figure 7(d) also shows that the graben M3 sinks with increase in Δ forming another crater on the right side of the horst M2. In other words, the rate of reduction of height of the graben is higher than that of the horst. Many field observations (e.g. Locat et al., 2011) show that the horsts projected up over the grabens after failure, as depicted in Fig. 1.

Conceptual models have been proposed in the past to explain the mechanisms of spread and retrogressive landslides (Odenstad, 1951; Carson, 1977, Carson, 1979b). These models describe the dislocation of the soil mass based on analysis of forces acting on the surfaces of horsts and grabens. Odenstad (1951) assumed that a horizontal weak surface or layer exists in the clay soil, and the strength of this weak layer is almost completely destroyed when the failure is initiated due to stress concentration. This model does not explain the formation and propagation of this horizontal shear band. In a recent study, Locat et al. (2013) took an initiative to model the propagation of the horizontal shear band. As mentioned in the introduction, although their FE models can simulate the propagation of a quasi-horizontal shear band, they could not simulate the whole process including the formation and displacement of horsts and grabens.

In the present FE model, the formation and propagation of shear bands are successfully simulated. The horizontal shear band (e.g. f_1 in Fig. 6) forms along the interface between the basal and sensitive clay layers. The other failure planes (e.g. f_2-f_6 in Fig. 6f) are not predefined, and therefore shear band formation occurs through stress concentrations and/or weaker zones due in part to stress redistribution and reduction of shear strength along the shear bands. At large Δ, a number of shear bands are formed above the initial horizontal shear band, which causes global failure of the slope and formation of horsts and grabens and finally spread failure. The simulation results suggest that the initial development and the extent of the horizontal shear band are important features to generate horsts and grabens in a progressive manner. The use of large deformation FE modeling technique coupled with strain/deformation dependent undrained shear strength model is one of the main advantages of the present FE model over the existing numerical models available in the literature.

FE Mesh Size

The size of the FE mesh has a significant influence on simulation results when the analyses involved with post-peak softening behavior of soil defined as a function of shear strain. Generally, for given relative displacements between two faces, the finer mesh calculates higher shear strain. Element size scaling rules have been proposed in the past to reduce the effects of mesh dependency (Pietruszczak and Mróz, 1981; Moore and Rowe, 1990; Andresen and Jostad, 2004; Anastasopoulos et al., 2007). In addition to the base case discussed in previous sections, analyses are also performed for two different mesh sizes (1.0 m and 0.25 m), again with uniform cubical elements in the whole domain. For FE input, γ^p is calculated scaling by element size; for example, s_{u95} mobilizes at $\gamma_{95}^p = \delta_{95}/t_{FE}$ of 3%, 6% and 12% for mesh size 1.0, 0.5 and 0.25 m,

respectively, for same δ_{95}=0.03 m. The orientation of the shear band is not considered in the scaling rule, which might induce some mesh dependency.

Figure 8 shows the shear bands, together with plastic shear strains, for three Δ values. Higher shear strains are calculated with finer mesh because $\gamma^p = \delta / t_{FE}$. Note that, for a better presentation of the shear bands, the adopted vertical scale is twice the horizontal scale in all the figures presented in the following sections. As shown in Figs. 8(a-c) for Δ=0.45 m, the length of the horizontal shear band is almost same ($\sim$68 m) for all three mesh sizes when the element size scaling rule is used. Analyses are also performed with the same value of $\gamma_{95}^p = 6\%$ (without element size scaling), which give 55, 68 and 88.5 m shear band length for the 1.0, 0.5 and 0.25 m meshes, respectively, at Δ=0.45 m. This shows that element size scaling significantly improves the simulation although the results are not strictly the same for these three mesh sizes. The shear bands at Δ=0.75 m are shown in Figs. 8(e-g). Again, the length of the shear bands and the location where the curved failure surface intersects the ground surface are consistent. Finally, Figs. 8(i-k) show the simulation results for a very large Δ (=17.25 m). The formation of shear bands with Δ shown in Figs. 8(i) and 8(j) is very similar, and has been discussed further in previous sections using Figs. 6 and 7. However, Fig. 8(k) shows that the 1.0 m mesh could not maintain the shape of the horsts and grabens at large displacements. From a close examination of the results it is found that the quasi-static conditions could not be maintained properly at this speed of the eroded block (v_e=0.05 m/s) in 1.0 m mesh. The effect is significant at large values of Δ because a large soil mass displaces at this stage resulting in increase of the kinetic energy. Therefore, in order to maintain quasi-static conditions, a simulation is also performed at a slower speed of the eroded block of v_e=0.01 m/s, and the results are shown in the last row of Fig. 8. As shown in Fig. 8(l), the shear bands formation at this v_e with 1.0 m coarse mesh is very similar to the shear bands formed in finer meshes (Figs.

16

8i & 8j). In other words, when the element size scaling is used, the results with these three different mesh sizes are comparable in terms of strain, displacement and shape of the displaced horst and grabens provided the quasi-static conditions are maintained. Analyses are also performed at a slower speed (v_e=0.01 m/s) for 0.25 m and 0.5 m mesh and the results are very similar to the first two rows in Fig. 8, which confirms that v_e=0.05 m/s is low enough to maintain quasi-static conditions for these two mesh sizes. It is to be noted here that this type of large deformation FE analysis is computationally expensive. Therefore, all the analyses presented in the previous and following sections are conducted with 0.5 m mesh and v_e=0.05 m/s.

Parametric Study

The geometry of the slope and soil parameters influence the shear band formation/propagation and spread failure. A parametric study is conducted using the above base case FE model in which only one parameter is varied while the other parameters are kept constant as listed in Table 1, unless otherwise mentioned.

Post-peak strength degradation parameter (δ_{95})

The undrained shear strength degradation occurs quickly if the value of δ_{95} in Eq. 1 is reduced. The analyses presented in the previous sections are for δ_{95}=0.03 m. In order to examine the effects of δ_{95}, analyses are also performed for δ_{95}=0.045, 0.1 and 0.15 m. Figure 9 shows the results for three different values of Δ. For δ_{95}=0.03, 0.045 and 0.1 m, a horizontal shear band forms with displacement of the eroded block as presented before in Fig. 6. A curved shear band is then formed, propagates upward and reaches the ground surface as shown in Figs. 9(a–c). Comparison of Figs. 9(a–c) shows that, for a given Δ, the length of the horizontal shear band increases with decrease in δ_{95}. The shear bands propagate faster for lower values of δ_{95} because of faster reduction of s_u. For

17

example, at Δ=22.35 m, two horsts and one graben are formed for δ_{95}=0.03 m (Fig. 9i) while only one horst and one graben are formed for δ_{95}= 0.1 m (Fig. 9k). The last row of Fig. 9 shows that the shear band formation with δ_{95}=0.15 m is different from other three rows. For δ_{95}=0.15 m, a curved shear band forms from the end of the horizontal shear band resulting in global failure of a large soil mass (Fig. 9d) as compared to other three cases (Figs. 9a–c). With further displacement of the eroded block, the failed soil mass disintegrated into smaller soil blocks as shown in Figs. 9(h) and 9(l), instead of formation of horst and grabens shown in Figs. 9(i–k). In summary, high brittleness (i.e. rapid decrease in s_u with δ) is required for formation of horsts and grabens. This is consistent with Locat et al. (2013) who also showed that brittle soils are more susceptible to progressive failure.

Slope angle (β)

The susceptibility and extent of progressive failure is high in steep slopes (Lo and Lee, 1973; Locat et al., 2013). In order to understand the mechanisms, analyses are performed for three different slope angles and the results are presented in Fig. 10. The thicknesses of the crust in all three cases are same as the base case shown in Fig. 3. As the value of β is different, the size of the eroded block is the largest for β=15° even though the maximum depth of excavation is same (10 m) in all three cases. Figure 10 shows the plastic strain contour for Δ=30.75 m. For β=15°, a horizontal shear band is formed that ended at 91 m from the crest. However for β=25°, a slightly shorter (89 m) horizontal shear band than that of β=15° is formed. In addition, some plastic shear strain accumulation above the horizontal shear band occurs as shown by the shaded zone near point A. It shows that there is a tendency to form another shear band even though it is not fully formed up

18

to the ground surface to cause a global failure as in the previous cases (e.g. failure of soil mass M1 in Fig. 6b). In both cases (β=15° and 25°), global failure of the slope does not occur, even though a large horizontal shear band is developed. It is to be noted here that additional triggering factors, such as construction in the upslope area, may cause a global failure as shown by the authors (Dey et al., 2014).

Unlike Figs. 10(a) and 10(b), a global failure occurs for β=30° (Fig. 10(c)) because the shear stress along the potential failure plane increases with the slope angle, β. The formation of horizontal shear band and subsequent horsts and grabens are discussed in detail in the previous sections. Based on this analysis, it can be concluded that the slope angle and the potential to initiate the first circular failure are the key factors for spread failure.

Sensitivity (S_t)

Figure 11 shows the effects of S_t on shear band formation. For a low S_t (=3), the post-peak reduction of s_u is not sufficient to cause global failure of the slope (Fig. 11a). With displacement of the eroded block a small horizontal shear band is formed and at one stage the eroded block separates from the remaining soil. For S_t=5 and 7, global failure and subsequent formation of horst and grabens occurs (Figs. 11(b) and 11(c)). The extent of failure increases with S_t because of higher reduction of s_u (compare Figs. 11b and 11c). However, the failure pattern is different if S_t is very high as shown in Fig. 11(d). In this case a large horizontal shear band is formed first with displacement of the eroded block. However, once the global failure is occurred by the formation of a curved shear band, strain concentration mainly occurs along the global failure plane instead of formation of horsts and grabens as shown in Figs. 11(b) and 11(c). Figure 11(d) also shows that,

19

although a large horizontal shear band is formed, the extent of failure is not visible at the ground surface, at least for the maximum displacement of the eroded block simulated in this case.

Thickness of crust and sensitive clay layer

In the analyses presented in previous sections, the thickness of the crust (H_c) and sensitive clay (H_{st}) are 3.0 m and 16.0 m, respectively (Fig. 3). Keeping the total thickness of soil above the base same (H_c+H_{st}=19.0 m), the effects of H_c and H_{st} on slope failure are investigated. Figure 12(a) shows that global failure of the slope does not occur when H_{st}=10.0 m because of existence of a thick crust (9.0 m) of higher shear strength, although a long horizontal shear band is formed. When H_{st}=14 or 16 m, global failure and subsequent formation of horst and grabens occur (Figs. 12(b) and 12(c)). Figure 12(b) shows the formation of shear bands f_1–f_6 in chronological order. Unlike Fig. 12(c), a shear band f_5 is formed in the sensitive clay layer just below the crust. The failure pattern shown in Fig. 12(d) for a very thin crust (H_c=1 m and H_{st}=18 m) is different from Figs. 12(b) or 12(c). In this case, although a large horizontal shear band is formed initially, horst and grabens do not form with displacement of the eroded block. Instead, large strain concentration mainly occurs around the global failure plane and only one block of failed soil mass follow the eroded block, at least, up to the maximum displacement of the eroded block simulated.

Shear strength of crust

Figure 13 shows that a horizontal shear band is formed initially for all three different values of undrained shear strength of the crust (s_{uc}). After the formation of first global failure plane, large deformation through the segment of the failure plane in the crust could occur easily for low s_{uc} (Fig. 13a) as compared to the simulations with high s_{uc} (e.g. Figs. 13(b) and 13(c)). Therefore, only one block of soil moves with the eroded block for s_{uc}=40 kPa. When the crust is relatively strong

(e.g. s_{uc}=60 or 80 kPa), the higher shear resistance in the segment of the failure plane in the crust results in formation of inclined downward shear bands in the sensitive clay layer (e.g. f_3 in Fig. 13c) and subsequent formation of horst and grabens (Figs. 13(b) and 13(c)). Similar to Fig. 12(b), a shear band f_5 is formed below the crust when s_{uc}=80 kPa, which suggest that the formation of such shear band depends upon thickness and strength of the crust.

Conclusions

Post slide field investigations of spreads in sensitive clay slopes show that in many cases a number of horst and graben blocks of almost intact clay displace laterally on a long flat horizontal failure plane. Early researchers assumed the presence of a hypothetical horizontal weak plane, and used this a priori failure plane to develop the conceptual models for spreads. In more recent studies, the formation of shear band due to disturbance at the toe of the slope and its propagation in the horizontal direction are modeled analytically and numerically for simplified conditions.

In the present study, the large deformation FE modeling technique in Abaqus CEL is used to simulate progressive failure. The development of horizontal shear band due to river bank erosion or excavation and its propagation in sensitive clay layer are simulated using a constitutive model that considers post-peak softening behaviour. In addition, successive formation of horsts and grabens with displacement of failed soil masses is successfully simulated. Very large displacement of the failed soil mass are simulated using Abaqus CEL without any numerical issues due to mesh distortion as encountered in typical FE modeling in Lagrangian framework. The parametric study shows that toe erosion does not always create horsts and grabens rather their formation depends on soil properties and geometry. The following conclusions can be drawn from this study:

21

i) Due to erosion or excavation near the toe of the slopes, a shear band could be formed and propagated horizontally in the sensitive clay to a large distance. The slope might be globally stable but the shear resistance in the band decreases to a low value.

ii) For the base case analysis, the first global failure occurs after the formation of a shear band above the initial horizontal shear band. The horsts and grabens are formed when the previous failed soil masses move a sufficiently large distance. Large plastic shear strains develop on the surfaces of horst and grabens, which reduces the undrained shear strength.

iii) When the stress-strain behaviour is defined by element size scaling rule, the simulation results are almost independent of mesh size, provided the quasi-static conditions are properly maintained during the analysis. Low speed of the eroded block is required to maintain quasi-static conditions for coarse mesh.

iv) The susceptibility and extent of progressive failure increase with decrease in δ_{95} because of quick post-peak reduction of undrained shear strength.

v) For the ground profile and soil properties considered in the bases case, a global failure does not occur for slope angles up to 25°, even though a large shear band develops. However, for slope angle of 30°, global failure and subsequent formation of horsts and grabens are simulated.

vi) For low values of S_t of sensitive clay layer, only a small horizontal shear band is formed by toe erosion. On the other hand, only one block of soil near the slope fails when S_t is very high. For intermediate values of S_t (5 and 7 in the present study) a number of horst and grabens are formed and the failure is extended over a large distance.

vii)   Toe erosion creates only a horizontal shear band when the crust is thick. For thin crust, global failure of only one soil block occurs. Horst and graben formation occurs only for intermediate thicknesses of the crust and sensitive clay layer. In addition to thickness, sufficiently high shear strength of the crust is required for the formation of horsts and grabens.

Finally, although a parametric study is performed for a number of soil parameters and geometry, the effects of other factors such as initial effective stress conditions, slope height, inclination of the ground surface, and the size and shape of the eroded block need to be investigated further.

Acknowledgements

List of symbols

The following symbols are used in this paper:

β slope angle

δ post-peak shear displacement

Δ displacement of the eroded block

δ_{95} δ at which s_u reduced by 95% of $(s_{up}\text{-}s_{uR})$

τ_c shear stress along the shear band

23

δ_e	elastic shear displacement
δ_p	plastic shear displacement
δ_{pc}	plastic shear displacement at point b in Fig.4
δ_t	total shear displacement
ν_u	undrained Poisson's ratio
L_{sb}^r	length of residual shear band where $\delta_p \geq (\delta_{pc}+\delta_{95})$
L_{sb}^s	Length of softening zone where $\delta_{pc}<\delta<\delta_{95}$
E_u	undrained modulus of elasticity
γ^p	plastic shear strain
H_c	thickness of crust (Fig. 3)
H_{st}	thickness of sensitive clay layer (Fig. 3)
H_b	thickness of the base (Fig. 3)
L_{ex}	lateral extent of failure
S_t	s_{up}/s_{uR}
s_u	mobilized undrained shear strength
s_{uc}	undrained shear strength of crust
$s_{u(ld)}$	s_u at large displacements
s_{up}	peak undrained shear strength
s_{uR}	s_u mobilized in shear band at considerable shear displacement
s_{ur}	s_u at completely remoulded state
t	shear band thickness
t_{FE}	finite element mesh size
v_e	speed of eroded block

References

Anastasopoulos, I., Gazetas, G., Bransby, M. F., Davies, M. C. R. and Nahas, A. El. (2007). Fault rupture propagation through sand: finite-element analysis and validation through centrifuge experiments. *J. of the Geotech. and Geoenviron. Eng.*, *ASCE*, **133**, No. 8, 943–958.

Andresen, L. and Jostad, H.P. (2004). Analyses of progressive failure in long natural slopes. *In Proc. of the 9th Symp. on Num. Models in Geomech. - NUMOG IX*, *Ottawa*, Ont., 603–608.

Anderson, L. and Jostad, H.P. (2007). Numerical modeling of failure mechanisms in sensitive soft clays — application to offshore geohazards. *Off. Technology Conf.*, *Texas,* OTC 18650.

Bernander, S. (2000). *Progressive failure in long natural slopes: formation, potential extension and configuration of finished slides in strain-softening soils*. Licentiate Thesis, Luleå University of Technology, Luleå, Sweden.

Bjerrum, L. and Landva, A. (1966). Direct simple-shear tests on a Norwegian quick clay. *Géotechnique*, **16,** No. 1, 1–20, http://dx.doi.org=10.1680=geot.1966.16.1.1.

Carson, M. A. (1977). On the retrogression of landslides in sensitive muddy sediments. *Canadian Geotechnical J.*, **14**, No. 4, 582–602.

Carson, M. A. (1979b). On the retrogression of landslides in sensitive muddy sediments: Reply. *Canadian Geotechnical J.*, **16**, No. 2, 431–444.

Demers, D., Robitaille, D., Locat, P., and Potvin, J. (2013). Inventory of large landslides in sensitive clay in the province of Quebec, Canada: preliminary analysis. *In Proc. of the 1st Int. Workshop on Landslides in Sensitive Clays,* Landslides in Sensitive Clays –From Geosciences to Risk Management, Québec, Que.

Dey, R., Hawlader, B., Phillips, R. and Soga, K. (2014). Stability analysis of a river bank slope with an existing shear band. *6th Canadian GeoHazards Conf.*, Kingston, Ontario.

Dutta, S., Hawlader, B. and Phillips, R. (2015). Finite element modeling of partially embedded pipelines in clay seabed using Coupled Eulerian–Lagrangian method. *Canadian Geotechnical Journal*, **52**, No. 1, 58–72, http://dx.doi.org= 10.1139/cgj-2014-0045.

Einav, I. and Randolph, M.F. (2005). Combining upper bound and strain path methods for evaluating penetration resistance. *Int. J. Num. Methods Engineering,* **63**, No. 14, 1991–2016.

Fortin, A., Ouellet, D., P aradis, S. and Demers, D. (2008). Développement au Ministère des Transports du Québec d'un porail informatique pour l'accès à des bases de données géotechnique. *In Proc. of the 4th Canadian Conf. on Geohazards*: F*rom Causes to Management, Québec*. Edited by J. Locat, D. Perret, D. Turmel, D. Demers, and S. Leroueil. Presses de l 'Université Laval, Québec, 169–174.

Fortin-Rhéaume, A.-A. (2013). *Étude de l'étalement latéral de 1988 et des autresglissements de terrain le long de la vallée a` Brownsburg-Chatham, Québec*. M.Sc. thesis, Département de génie civil, Université Laval, Québec.

Griffiths, D. V. and Lane, P. A. (1999). Slope stability analysis by finite elements. *Géotechnique*, **49**, No. 3, 387–403, http://dx.doi.org=10.1680=geot.1999.49.3.387.

Grondin, G., and Demers, D. (1996). The Saint-Liguori flake slide: characterization and remedial works. *In Proc. of the 7th Int. Symposium on Landslides*, *Trondheim, Norway*. Edited by K. Senneset. Balkema, Rotterdam, the Netherlands, **2**, 743–748.

Gauer, P., Kvalstad, T. J., Forsberg, C. F., Bryn, P., and Berg, K. (2005). The last phase of the Storegga Slide: simulation of retrogressive slide dynamics and comparison with slide-scar morphology. *Marine and Petroleum Geology*, **22**(1-2): 171–178.

Gylland, A. S., Sayd, M. S., Jostad, H. P., and Bernander, S. (2010). Investigation of soil property sensitivity in progressive failure. *In Proc. of the 7ᵗʰ European Conf. on Num. Methods in Geotech. Eng.*, Trondheim, Norway, 515–520.

Jostad, H. P., and Andresen, L. (2002). Capacity analysis of anisotropic and strain-softening clays. *In Proc. of NUMOG VIII*, Rome, Italy, 469–474.

Karlsrud, K., Aas, G. and Gregersen, O. (1984). Can we predict landslide hazards in soft sensitive clays? Summary of Norwegian practice and experiences. *In Proc. of the 4th Int. Symposium on Landslides,* Toronto, Ont., **1**, 107–130.

Kvalstad, T.J., Andresen, L., Forsberg, C.F., Berg, K., and Bryn, P. (2005). The Storegga Slide: evaluation of triggering sources and slide mechanisms. Marine and Petroleum Geology, **22**(1-2): 245–256.

Leroueil, S. (2001). Natural slopes and cuts: movement and failure mechanisms. *Géotechnique,* **51**, No. 3, 197–243, http://dx.doi.org=10.1680=geot.2001.51.3.197.

Lo, K.Y., and Lee, C.F. (1973). Stress analysis and slope stability in strain-softening soils. *Géotechnique*, **23**, No. 1, 1–11, http://dx.doi.org=10.1680=geot.1973.23.1.1.

Locat, A. (2007). *Étude d'un étalement latéral dans les argiles de l'Est du Canada et de la rupture progressive, Le cas du glissement de Saint-Barnabé-Nord*. M.Sc. thesis, Département de génie civil, Université Laval, Québec, Que.

Locat, A., Leroueil, S., Bernander, S., Demers, D., Locat, J. and Ouehb, L. (2008). Study of a lateral spread failure in an eastern Canada clay deposit in relation with progressive failure: the Saint-Barnabé-Nord slide. *In Proc. of the 4th Canadian Conf. on Geohazards: From Causes to Management,* Québec, Que., 89–96.

Locat, A., Leroueil, S., Bernander, S., Demers, D., Jostad, H.P. and Ouehb, L. (2011). Progressive failures in eastern Canadian and Scandinavian sensitive clays. *Canadian Geotechnical J.,* **48**, No. 11, 1696–1712.

Locat, A., Jostad, H. P. and Leroueil, S. (2013). Numerical modeling of progressive failure and its implications for spreads in sensitive clays. *Canadian Geotechnical J.*, **50**, No. 9, 961–978.

Loukidis, D., Bandini, P., and Salgado, R. (2003). Stability of seismically loaded slopes using limit analysis. *Géotechnique*, **53**, No. 5, 463–479, http://dx.doi.org=10.1680=geot.2003.53.5. 463.

Moore, I. D. and Rowe, R. K. (1990). Scaling rule for localized plasticity in strain-softening continua. *Proc. of 1st Int. Conf. on Computer Aided Assessment of Localized Damage, Portsmouth*, **2**, 99–112.

Odenstad, S. (1951). The landslide at Sköttorp on the Lidan River, February 2, 1946. *Royal Swedish Institute Proceedings*, **4,** 1–38.

Palmer, A. C., and Rice, J. R. (1973). The growth of slip surfaces in the progressive failure of overconsolidated clay. *Proc. R. Soc. London, Ser. A*, **332**, No. 1591, 527–548.

Pietruszczak, St. and Mróz, Z. (1981). Finite element analysis of deformation of strain-softening materials. *Int. Journal for Numerical Methods in Engineering*, **17**, No. 3, 327–334.

PLAXIS. (2011). PLAXIS 2D 2010 manuals. PLAXIS bv., Delft, the Netherlands.

Potts, D. M., Dounias, G. T., and Vaughan, P. R. (1990). Finite element analysis of progressive failure of Carsington embankment, *Géotechnique,* **40**, No. 1, 79–101, http://dx.doi.org=10. 1680=geot.1990.40.1.79.

Puzrin, A. M., Germanovich, L. N. and Kim, S. (2004). Catastrophic failure of submerged slopes in normally consolidated sediments. *Géotechnique,* **54**, No. 10, 631–643, http://dx.doi.org=10. 1680=geot.2004.54.10.631.

Puzrin, A. M. and Germanovich, L. N. (2005). The Growth of Shear Bands in the Catastrophic Failure of Soils. *Proc. R. Soc. London, Ser. A*, **461**, No. 2056, 1199–1228.

Qiu G, Henke S, Grabe J. (2011). Application of a Coupled Eulerian–Lagrangian approach on geomechanical problems involving large deformations. *Computers and Geotechnics*, **38** No. 1, 30–39.

Quinn, P., Diederichs, M.S., Hutchinson, D.J. and Rowe, R.K. (2007). An exploration of the mechanics of retrogressive landslides in sensitive clay. *In Proc. of the 60th Canadian Geotechnical Conf.*, Ottawa, Ontario, 721–727.

Quinn, P. (2009). *Large Landslides in Sensitive Clay in Eastern Canada and the Associated Hazard and Risk to Linear Infrastructure*. Doctoral thesis, Queen's University, Kingston, Ontario, Canada.

Quinn, P. E., Diederichs, M. S., Rowe, R. K. and Hutchinson, D. J. (2011). A new model for large landslides in sensitive clay using a fracture mechanics approach. *Canadian Geotechnical J.*, **48**, No. 8, 1151–1162.

Quinn, P. E., Diederichs, M. S., Rowe, R. K., and Hutchinson, D. J. (2012). Development of progressive failure in sensitive clay slopes. *Canadian Geotechnical J.*, **49**, No. 7, 782–795.

Tavenas, F., Flon, P., Leroueil, S. and Lebuis, J. (1983). Remolding energy and risk of slide retrogression in sensitive clays. *Proc. of the Symposium on Slopes on Soft Clays,* Linköping, Sweden, SGI Report No. **17,** 423–454.

Tavenas, F. (1984). Landslides in Canadian sensitive clays — a state-of the-art. *In Proc. of the 4th Int. Symposium on Landslides*, Toronto, Ont., **1,** 141–153.

Tho, K. K., Leung, C. F., Chow, Y. K., and Swaddiwudhipong, S. (2012). Eulerian finite element technique for analysis of jack-up spudcan penetration. *ASCE International Journal of Geomechanics*, **12**, No. 1, 64–73.

Tian, Y., Wang, D., and Cassidy, M. J. (2011). Large deformation finite element analysis of offshore penetration tests. *Proc 2nd Int Symp Comput Geomech, Cavtat-Dubrovnik,* 925–933.

Wang, D., Randolph, M. F. and White, D. J. (2013). A dynamic large deformation finite element method based on mesh regeneration. *Computers and Geotechnics*, **54**, 192–201.

Figure 1: Typical morphology of spreads – The 1989 landslide at Saint-Liguori, Quebec (Locat et al., 2011)
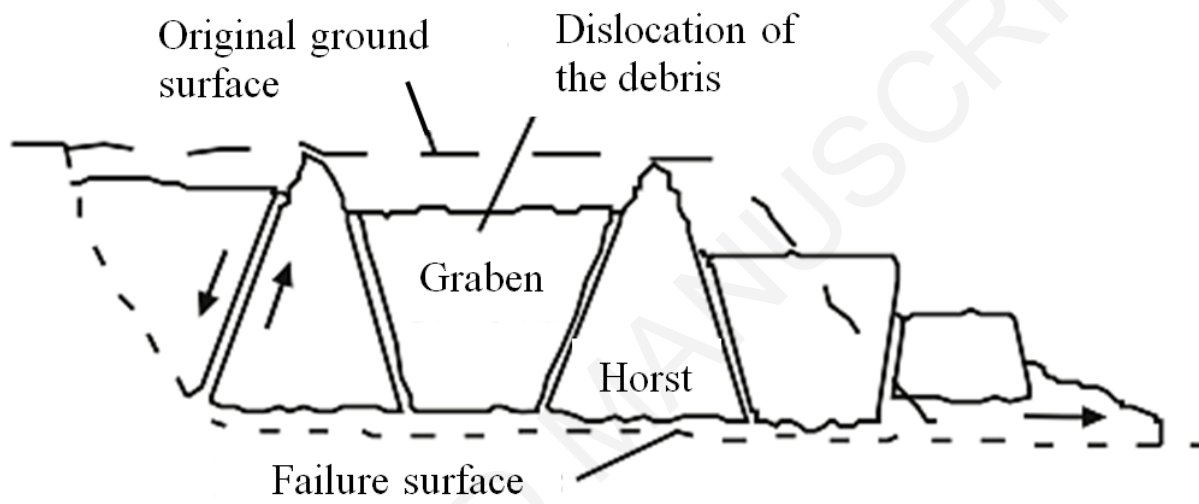
Figure 2: Sketch of spread type landslide in sensitive clay (after Locat et al. 2013)
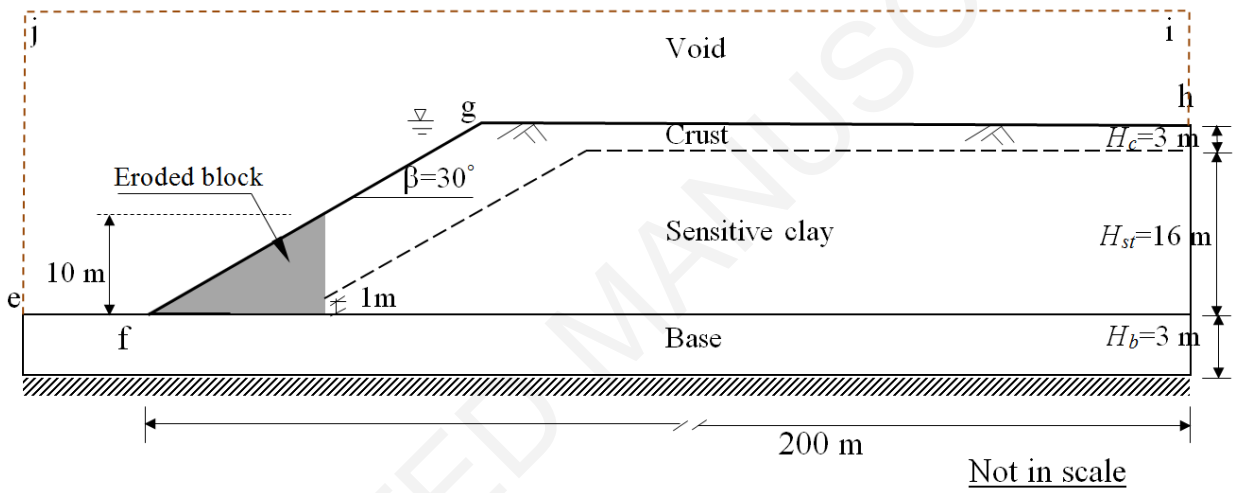
Figure 3: Geometry of the "base case" slope used in numerical analysis
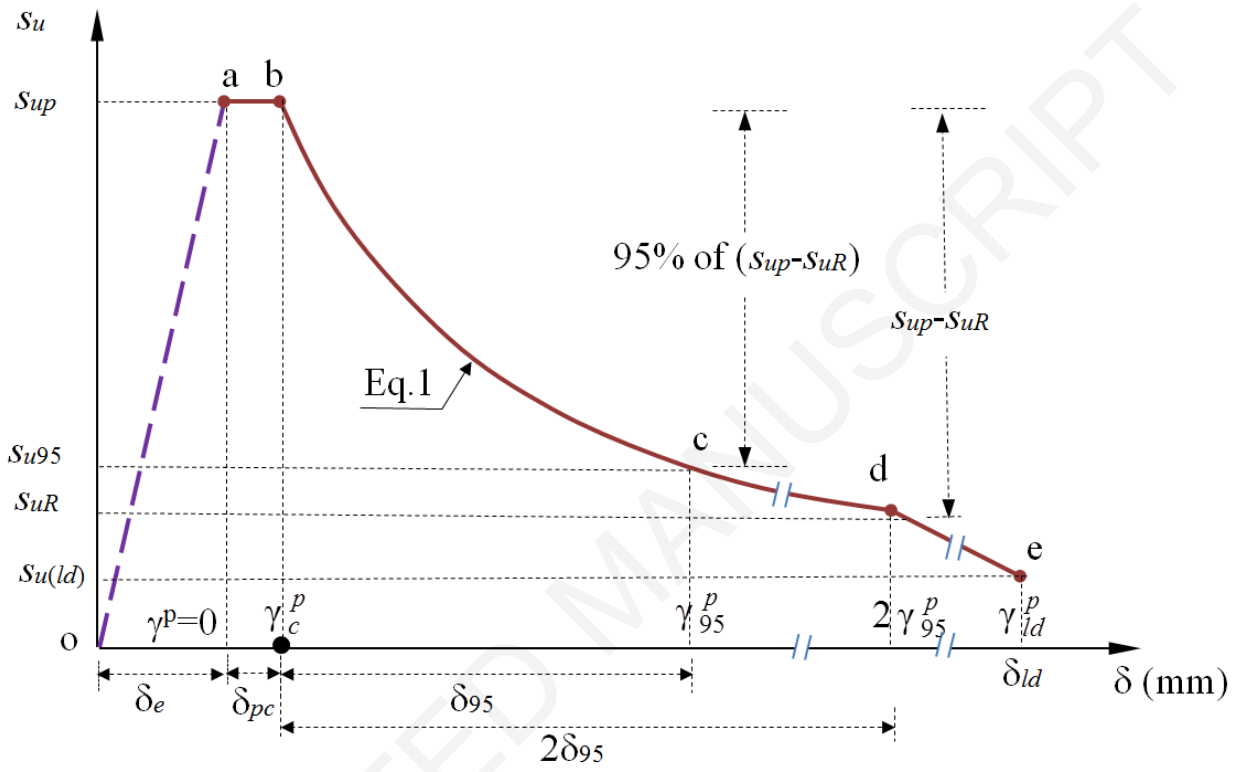
Figure 4: Stress-strain behavior used in finite element modeling
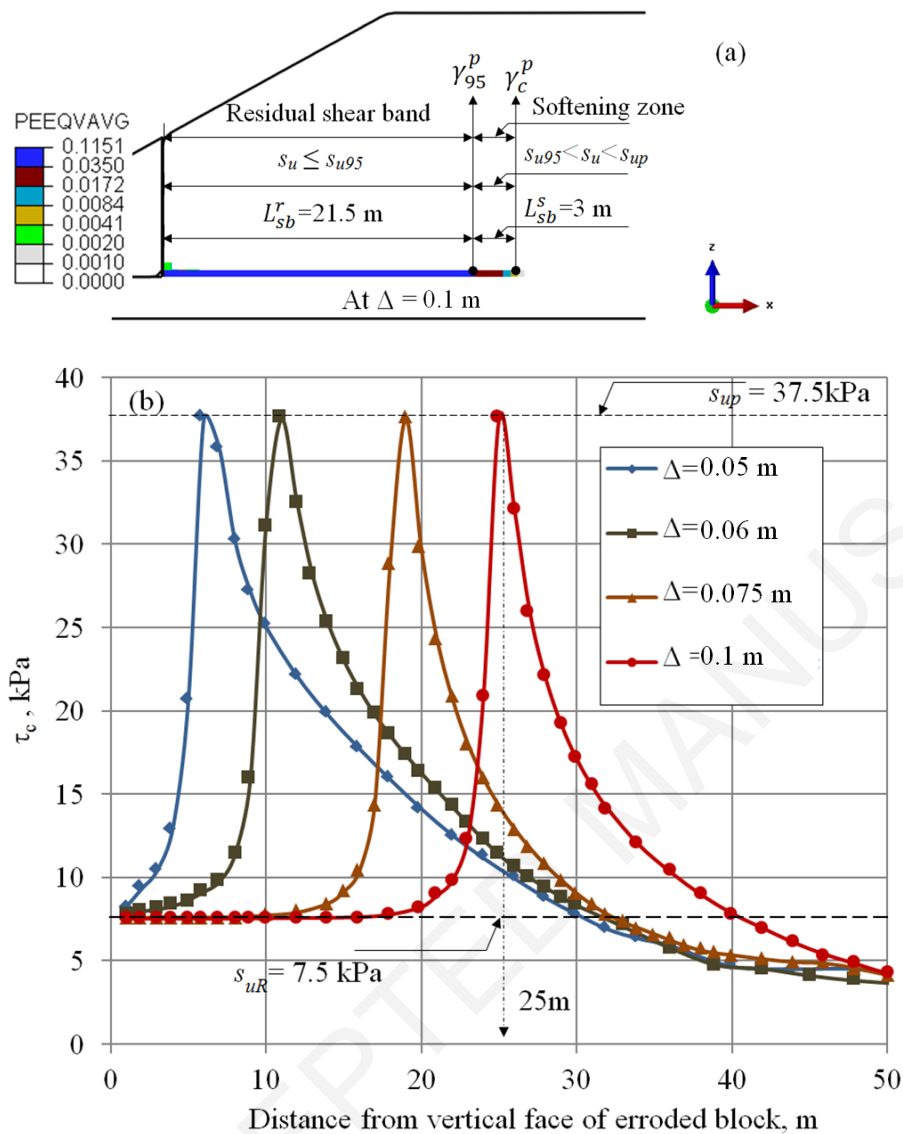
Figure 5: Mobilized stress and strain in shear band: (a) equivalent plastic shear strain at Δ=0.1 m, (b) Shear stress
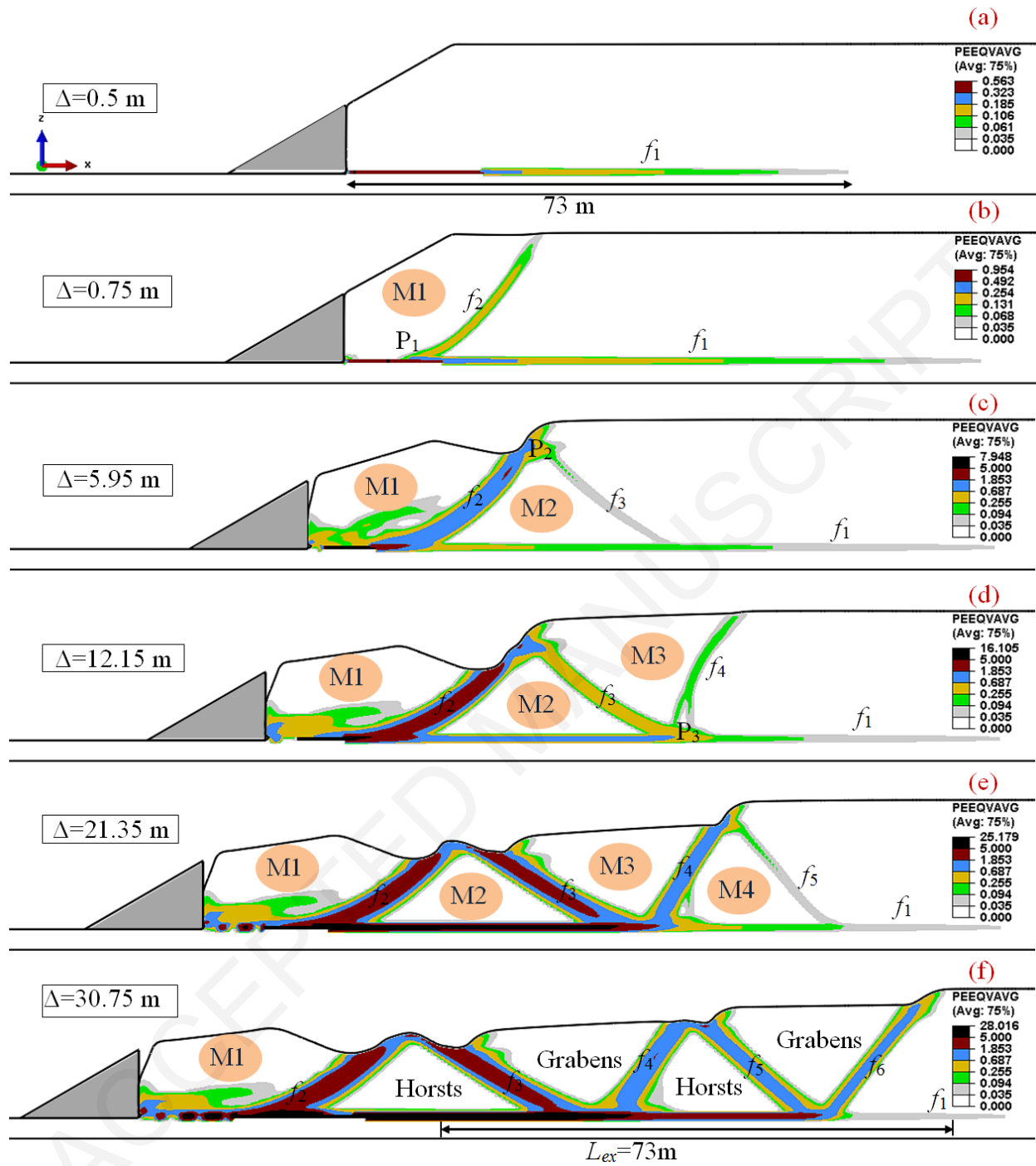
Figure 6: Formation of horsts and grabens leading to spread
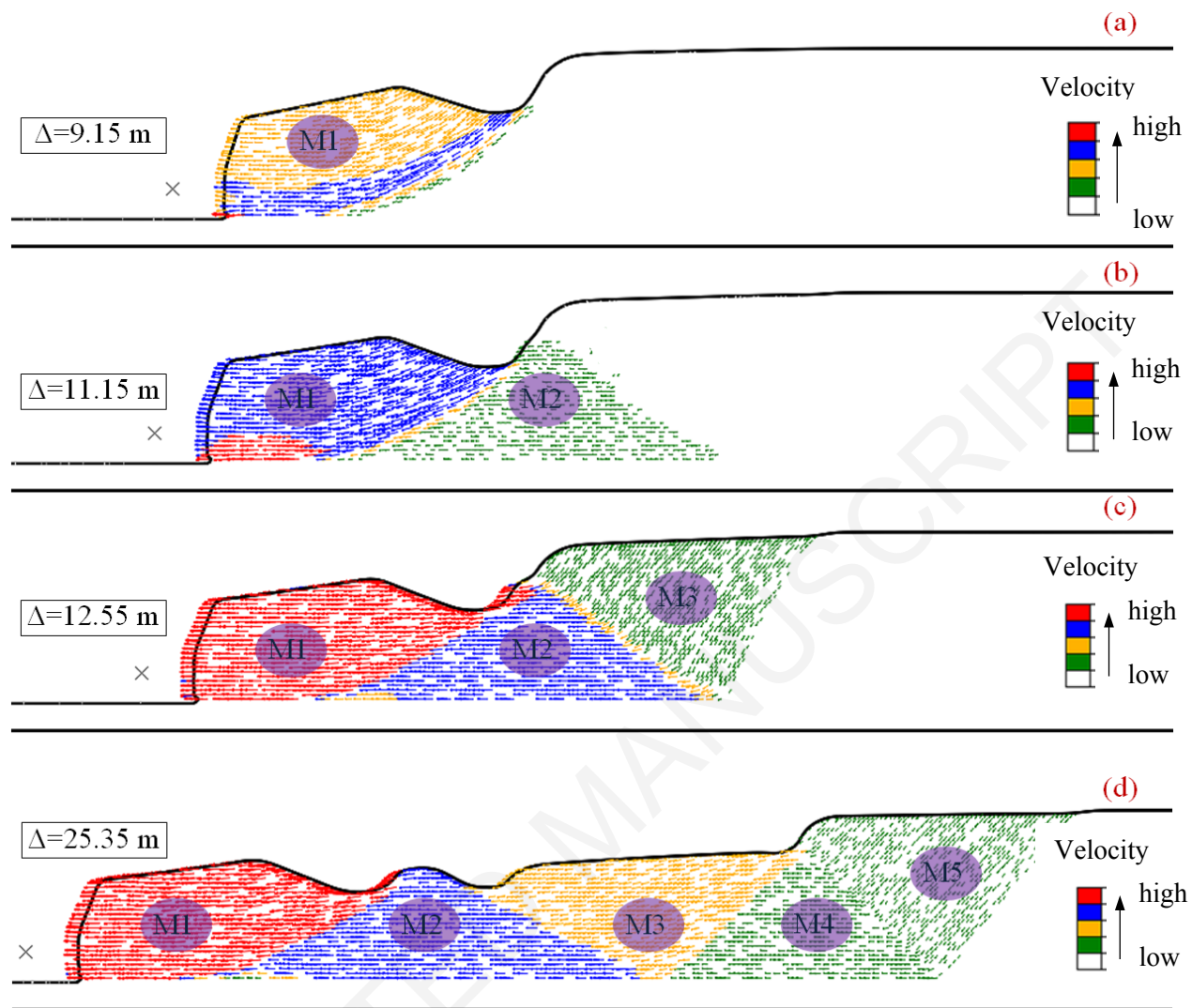
Figure 7: Velocity vectors of soil elements
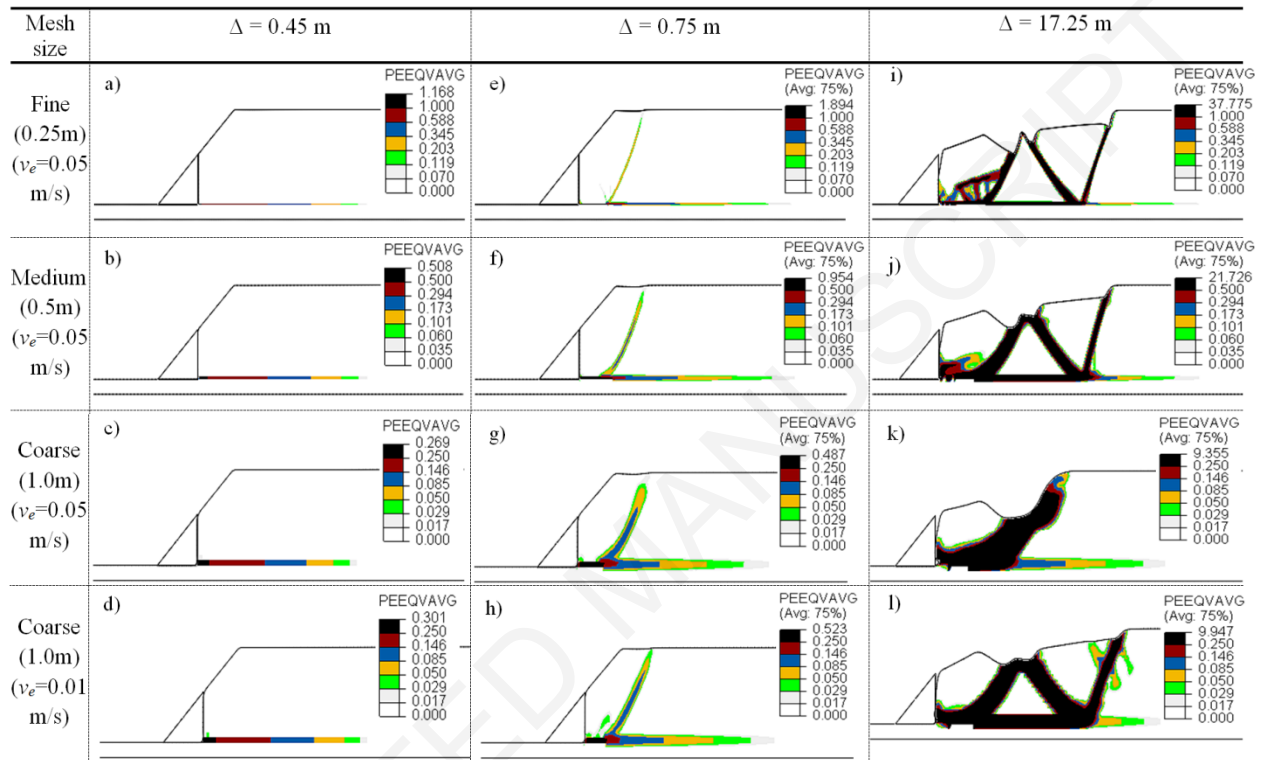
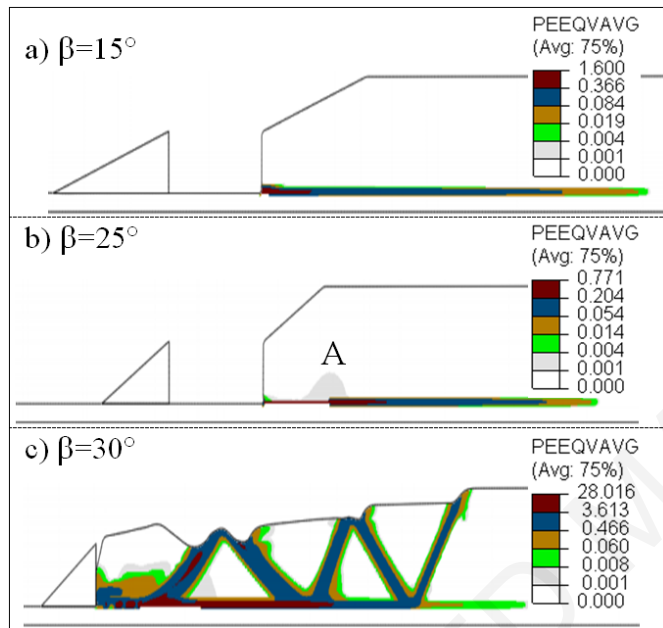Figure 8: Effects of mesh size on development of shear bands
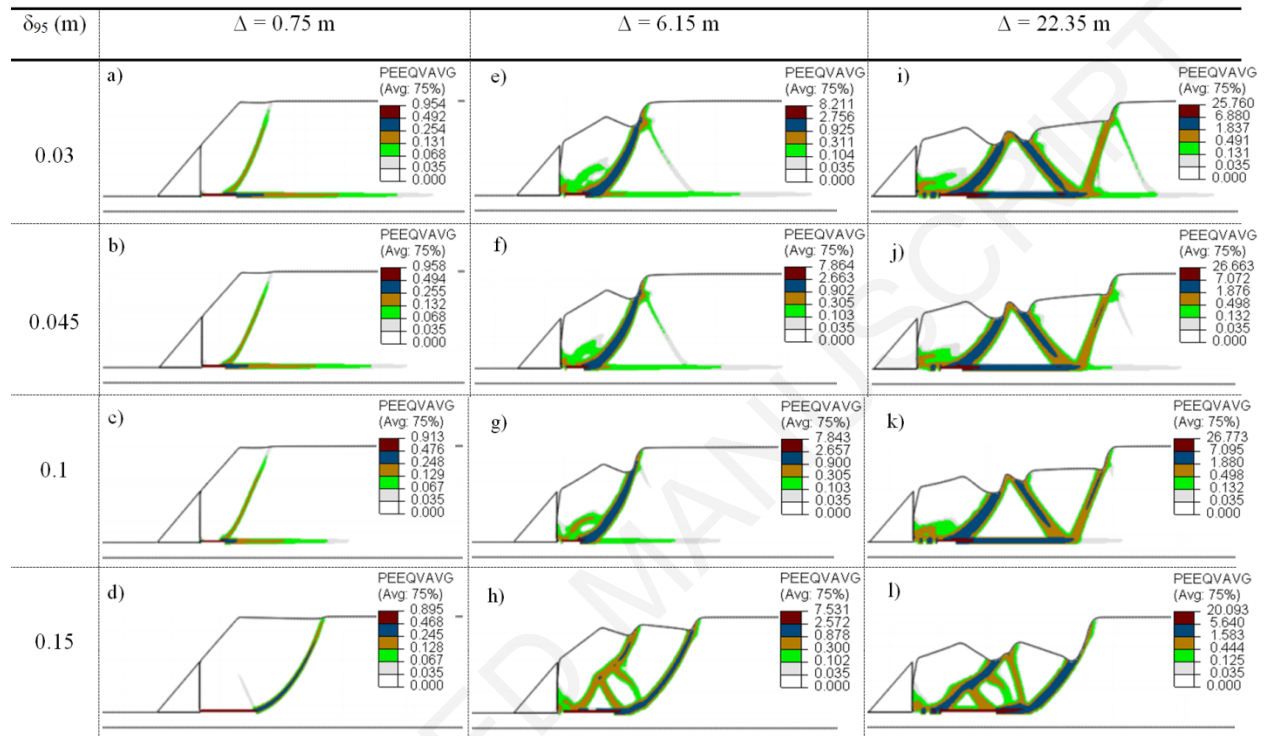
Figure 9: Effect of δ_{95}

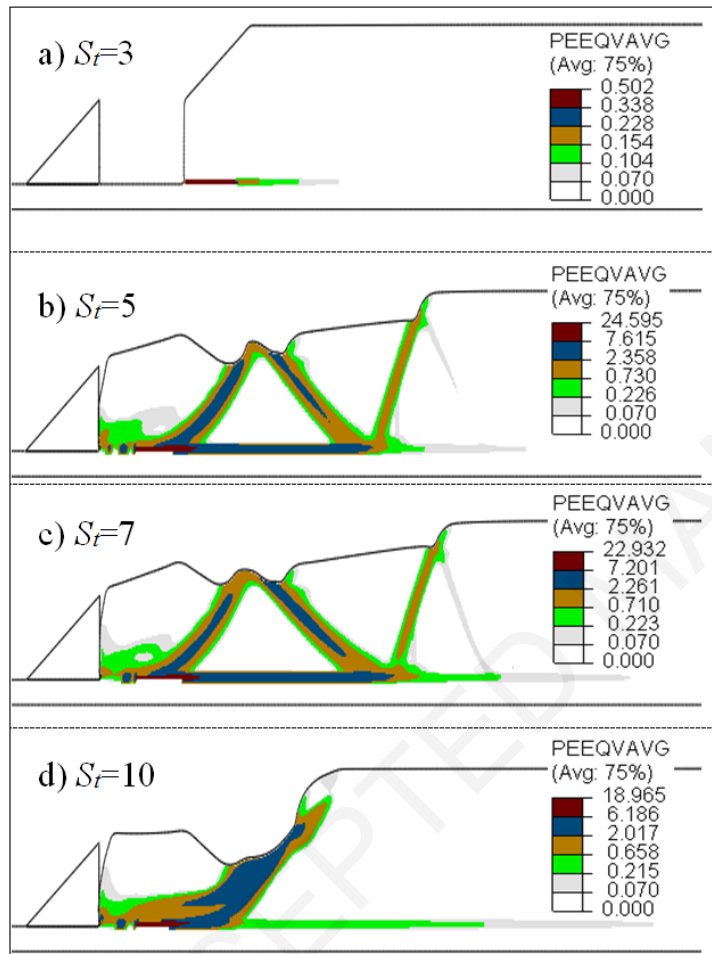Figure 10: Effect of river bank slope angle (β) at Δ=30.75 m
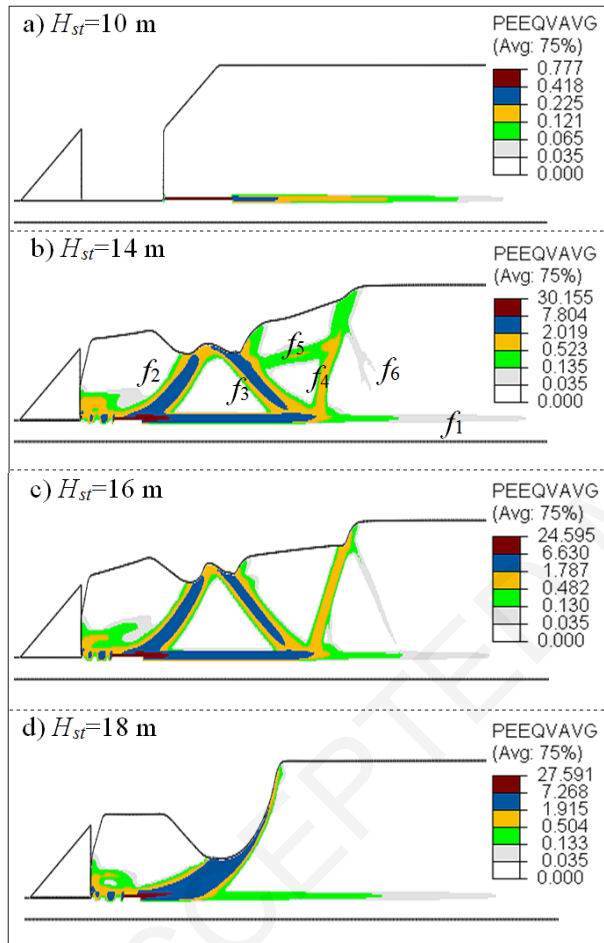
Figure 11: Effects of sensitivity at Δ=20.5 m

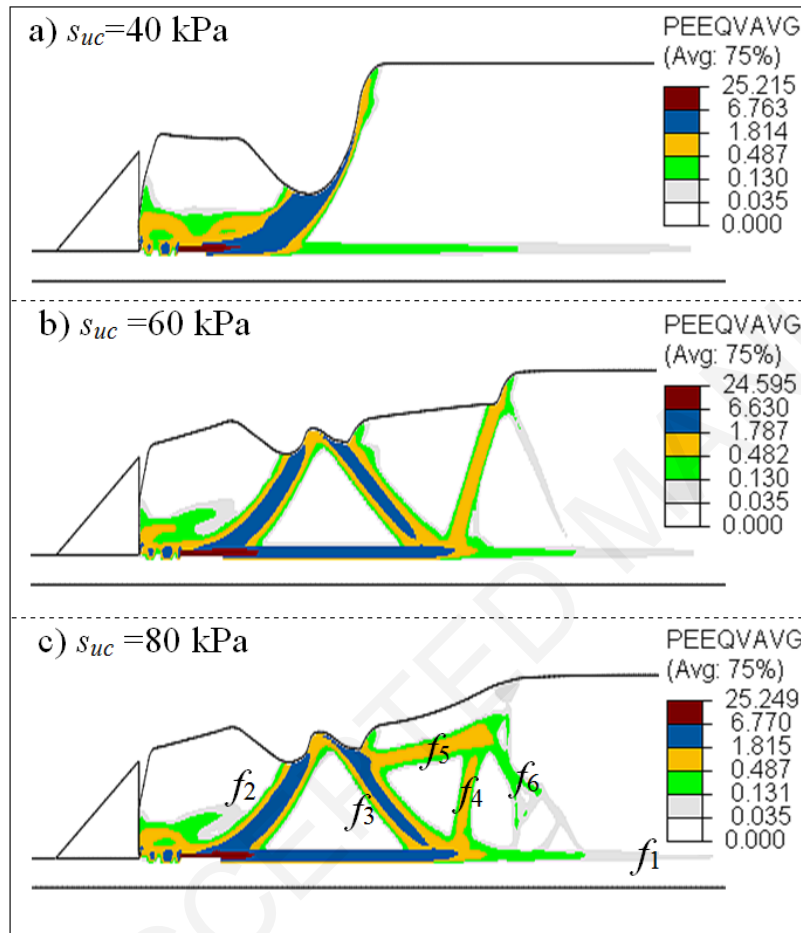Figure 12: Effect of crust and sensitive clay layer thickness at Δ=20.55 m

Figure 13: Effect of undrained shear strength of the crust (s_{uc}) at $\Delta=20.55$ m

Table 1: Parameters used for finite element modeling

Parameters	Values		
	Sensitive clay	Crust	Base
Undrained Young's modulus, E_u (MPa)	7.5	10	100
Poisson's ratio, ν_u	0.495	0.495	0.495
Peak undrained shear strength, s_{up} (kPa)	37.5	60[*]	-
Undrained shear strength, s_{uR} (kPa)	7.5	-	-
Large displacement undrained shear strength, $s_{u(ld)}$ (kPa)	2.0	-	-
δ_{pc} (m)	0.004	-	-
δ_{95} (m)	0.03	-	-
δ_{ld} (m)	2.0	-	-
Submerged unit weight, γ' (kN/m³)	8.0	9.0	11

[*]crust is modeled as elastic-perfectly plastic without softening